

Ink Jet Printing for Direct Mask Deposition in Printed Circuit Board Fabrication

Wen-Kai Hsiao, Stephen D. Hoath[^], Graham D. Martin[^] and Ian M. Hutchings
Department of Engineering, University of Cambridge, Cambridge, United Kingdom CB3 0FS
E-mail: wkh26@cam.ac.uk

Abstract. Drop deposition has been studied over a wide range of time scales under conditions relevant to direct printing of etch resist patterns on printed circuit boards. Early-stage impact-driven spreading of 80 pl drops of UV ink and phase change resist was imaged by 20 ns duration flash-based photography, while a 27,000 fps high-speed camera was used to study the later stages of spreading up to 130 ms postimpact. The presence of an attached ligament at impact was shown to reduce the effect of impact inertia and the tendency for recoil, although this was less significant in the later, capillary phase. The effects of surface wetting appeared to be insignificant during the impact and relaxation spreading phases but dominated the behavior during capillary spreading. Cooling by conduction from the substrate was shown to be effective in arresting drop spreading for the phase-change ink on a submillisecond time scale. © 2009 Society for Imaging Science and Technology.
[DOI: 10.2352/J.ImagingSci.Technol.2009.53.5.050304]

INTRODUCTION

Modern consumer and commercial electronics are built around printed circuit boards (PCBs). The low cost and high component density achievable with PCBs are essential in the relentless drive for miniaturization and affordability. Fabrication of PCBs is currently a multi-step process involving photolithographic masking and etching of the copper-clad laminated boards to create conductive tracks. This process not only utilizes costly equipment but is also inflexible to design changes and adapts poorly to variations in process parameters (e.g., to compensate for board distortion). There is, therefore, a growing interest in introducing ink jet printing techniques as an alternative to the conventional PCB manufacturing process. Etch resist masks can be printed directly on to Cu-clad laminated boards using jettable resist inks, eliminating multiple masking and alignment steps. An ink jet-based PCB fabrication process not only eliminates expensive masks and associated photolithographic equipment, but the inherent digital nature of ink jet printing also greatly improves the design flexibility as well as allowing for in-line correction of board distortion and other process variations. The traditional and ink jet-based PCB manufacturing processes are compared schematically in Figure 1.

Although ink jet printing is a relatively mature tech-

nique for graphical applications, our understanding of much of its governing physics, specifically in terms of drop deposition behavior, is far from complete. As a result, mask printing by ink jet printing often produces unsatisfactory results, as shown in Figure 2. The deterioration of the print quality is mainly attributed to uncontrolled spreading after ink deposition. However, the effects on drop spreading of drop deposition dynamics under the conditions of ink jet printing have not been studied in detail. Ink drops ejected from a print head nozzle often have attached ligaments up to ~1 mm in length.¹ With the short printing distance characteristic of high precision printing, such drops tend to deposit with these ligaments still attached. The effects of attached ligaments on drop deposition have not, to the best of the authors' knowledge, been studied before. In addition, the excessive spreading of ink drops deposited on nonabsorbent, high-energy metallic surfaces has not been quantified over the appropriate dimensional and time scales. Finally, the effect of substrate temperature on ink jet-sized drop spreading needs to be quantified when printing phase-change inks such as hot melt etch resists.

Although the impact of liquid drops on solids has been extensively studied since Worthington's pioneering studies more than 130 years ago,² the ability to study drop impact at ink jet length scales is constrained by the very small drop volume and very short event time scale. The following sections will first present an analysis of the physical processes which relate to the effects of fluid ligaments, substrate wetting, and temperature on ink jet drop deposition. By using both short-duration flash photography and high-speed

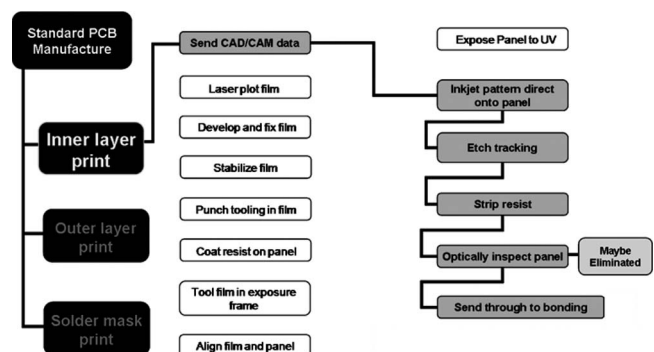


Figure 1. Ink jet-based PCB fabrication flow chart showing eliminated photolithographic steps (courtesy of Printed Electronics Ltd, UK).

[^]IS&T Member.

Received Dec. 23, 2008; accepted for publication Jun. 12, 2009; published online Aug. 27, 2009.

1062-3701/2009/53(5)/050304/8/\$20.00.

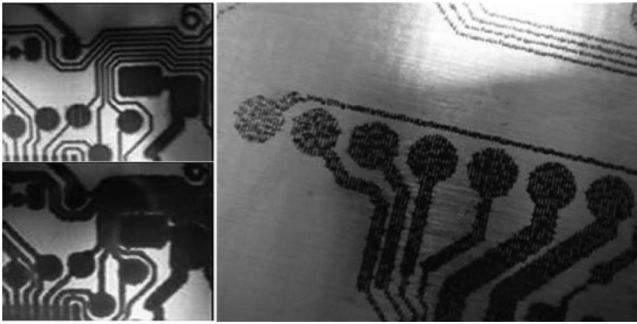


Figure 2. Poor quality samples of ink jet-printed PCB masks (courtesy of Printed Electronics Ltd, UK).

video to image the impact and spreading behavior of ink drops on PCB substrates, these analytical assumptions can then be verified. The objective of the work is to demonstrate both methodology and apparatus that can be used to investigate ink jet scale drop deposition behavior in order to generate data for the development of next generation ink jet-based manufacturing processes.

DROP DEPOSITION PROCESS

Postimpact drop deformation and spreading are controlled by fluid inertia, capillary force, and viscous dissipation. These phenomena are conveniently characterized by dimensionless parametric groups such as the Weber number (We), Ohnesorge number (Oh), and Reynolds number (Re) which are defined as follows:

$$\begin{aligned}
 We &= \frac{\rho U_o^2 D_o}{\sigma}, \\
 Oh &= \frac{\mu}{\sqrt{\rho \sigma D_o}}, \\
 Re &= \frac{\rho U_o D_o}{\mu} = \frac{\sqrt{We}}{Oh}, \quad (1)
 \end{aligned}$$

where ρ , σ , μ , D_o , and U_o are the liquid density, surface tension, dynamic viscosity, initial drop diameter, and impact velocity, respectively. The dynamics of drop spreading can be characterized primarily by the Weber and Ohnesorge numbers, as shown in Figure 3 (adapted from Schiaffino and Sonin³). The value of We determines the origin of the driving force for spreading, while Oh describes the force that resists spreading. The conditions for ink jet printing lie in a regime where, at least for the earlier stages of impact, inertial forces dominate and viscous forces are weak. As the spreading liquid comes to rest, however, capillary (surface tension) forces become more important.⁴ Few published droplet deposition studies have been conducted specifically in the parametric regime which is relevant to ink jet printing.⁵⁻⁸ Splashing on impact is unlikely for a drop deposited by drop-on-demand (DoD) printing when there is insufficient impact inertia to distort and fracture the spreading liquid

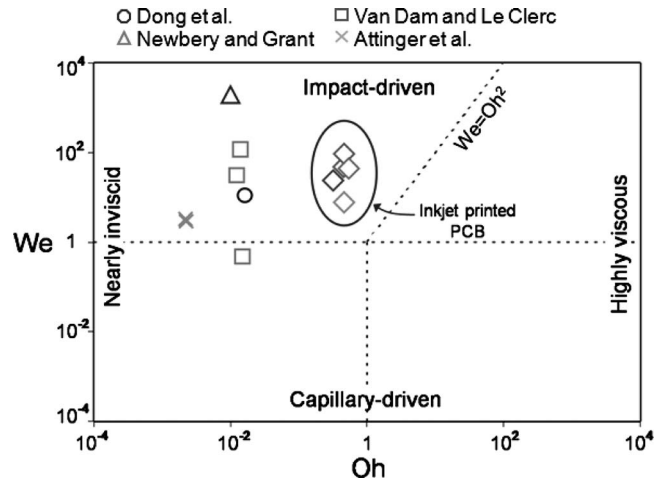


Figure 3. Map showing regimes of drop behavior on impact (adapted from Ref. 3) with the conditions used in the present work indicated.

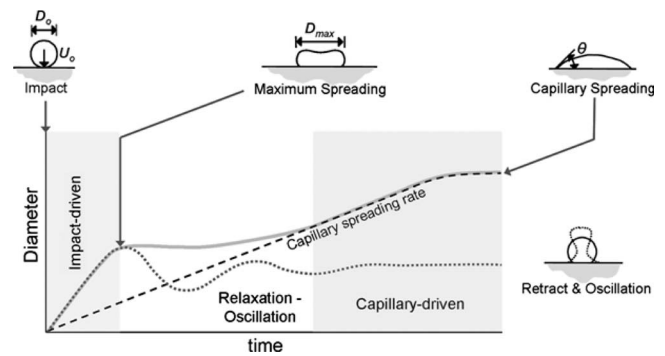


Figure 4. Phases of drop deposition process.

front, and the predominant behavior is generally well-damped spreading with minimal or no oscillation.

For an ink drop deposited on to a nonabsorbing, inert and rigid surface with negligible roughness, the extent of its spreading after impact can be described by its normalized contact diameter: $D^* = D(t)/D_o$. Figure 4 illustrates schematically how the contact diameter evolves with time. There are generally three distinct phases which can be described in terms of the progressive influences of inertia and capillary forces:⁹

- (1) The impact phase: in which inertia deforms the deposited drop and forces the liquid to spread away from the point of impact. The radial expansion is resisted by both surface tension and liquid viscosity. Both the spreading rate and the diameter of the deposited drop during this phase depend strongly on the impact parameters.
- (2) The relaxation phase: when the impact inertia is dissipated completely at the end of the impact driven stage, the deposited drop pauses momentarily. Depending on the extent of the initial spreading and surface wetting, the drop will either experience hysteresis at the contact line (i.e., the contact angle varies while the contact line remains stationary) or oscillation and retraction.

- (3) The capillary phase: while both the impact and relaxation phases can be regarded as responses to drop impact conditions, the final phase is dominated by the liquid-surface capillary effect, or wetting. On a wetting surface, the deposited drop may continue to spread beyond the limit reached during the impact phase. On the other hand, spreading may be arrested or even reduced on a nonwetting surface.

Drop Spreading Distances

There are several variables describing the evolution of a deposited drop that are useful when developing an ink jet-based PCB fabrication process. Dimensions such as the maximum spread diameter at the end of the impact phase, D_{\max} , and the equilibrium spread diameter, D_{equ} , are valuable as they can potentially be used to predict printed line width and the maximum achievable print resolution. As no analytical solution exists for the transient free surface motion in the initial, impact-driven drop spreading phase, most estimations of D_{\max} are based either on energy conservation with considerations of viscous dissipation and contact angle dynamics^{10–14} or on empirical correlations.^{15,16} While an analytical prediction may be preferable for its versatility, comprehensive models similar to that of Roisman et al.¹⁴ require the dynamic contact angle to be determined during spreading, which is inconvenient when developing manufacturing processes. On the other hand, Dong et al.⁷ compared a range of model predictions with their experimental results and found good agreement with the empirical correlation of Scheller and Bousfield,¹⁶

$$D_{\max}^* = \frac{D_{\max}}{D_o} = 0.6 \left(\frac{We}{Oh} \right)^{0.166}, \quad (2)$$

despite the fact that it ignores liquid-surface interaction, i.e., wetting. This is perhaps not surprising as the initial process of drop spreading is dominated by inertia, a hypothesis supported by Asai's observation, for impact on various grades of paper and plastic films that the maximum spreading of an ink jet drop was surface independent.¹⁵

If the sessile drop acquires a spherical cap shape, the nondimensional equilibrium diameter after spreading may be predicted simply from:

$$D_{\text{equ}}^* = \frac{D_{\text{equ}}}{D_o} = \frac{2}{[\tan^3(\theta/2) + 3 \tan(\theta/2)]^{1/3}}, \quad (3)$$

where θ is the equilibrium contact angle.

While both D_{\max}^* and D_{equ}^* can be used to characterize the spreading of a drop, the significance of these quantities in process development also depends greatly on the relevant time scales at which they are attained since techniques such as UV pinning, cooling, or even solidification can be used to slow down or arrest spreading. Therefore, the time scales involved in drop spreading also need to be understood.

Drop Spreading Time Scale

The various times involved, such as the duration of the impact phase, the time scale of the relaxation phase, and the spreading rate during the capillary phase are all relevant to an ink jet-based PCB fabrication process. For example, comparison of the duration of the impact phase, t_p , with the ink curing time will determine whether the distance D_{\max} limits the print resolution. Pasandideh-Fard et al.¹¹ estimated analytically the time required to reach D_{\max} by assuming that the drop spreads into a cylindrical disk upon impact. By considering the liquid to be incompressible and nonevaporating and hence to have constant volume, they estimated the duration to be $\frac{8}{3}(D_o/U_o)$. This estimate has been validated for the ink jet regime by reported experimental values for the deposition of μm -sized drops.⁵ For a typical DoD drop with a diameter of 50 μm deposited at 5 m/s, the duration of the impact phase can thus be estimated as $\sim 30 \mu\text{s}$.

Distorted by the impact inertia, the shape of the deposited drop approximates a cylindrical disk at the end of the impact phase. While the drop is momentarily at rest, this configuration incurs an excess of surface energy. Therefore, the drop will have a tendency to return to a lower energy configuration during the relaxation phase. If the initial distortion is severe, this "restoration" may cause oscillation or even retraction of the contact line. The behavior of a drop during the relaxation phase is characterized by its tendency to oscillate, scaled by the free oscillation period of a liquid drop,

$$t_{\text{osc}} = \sqrt{\frac{\rho D_o^3}{\sigma}}, \quad (4)$$

and the time scale for viscous decay,

$$t_{\text{damp}} = \frac{\rho D_o^2}{\mu}. \quad (5)$$

The ratio between the oscillation period and the viscous damping time

$$\frac{t_{\text{damp}}}{t_{\text{osc}}} = \frac{\sqrt{\rho D_o \sigma}}{\mu} = \frac{1}{Oh} \quad (6)$$

defines the oscillation response of the deposited drop.³ For typical DoD printing conditions, this ratio is $\sim 1.5 - \sim 3$ which indicates a well-damped oscillation. Therefore, an order-of-magnitude estimate of the duration of the relaxation period, t_r , can be made from the half period of the viscous damping time, which will be approximately 70–100 μs for typical ink jet printing conditions.

Following the relaxation phase, drop spreading is controlled by the capillary force acting along the contact line. Capillary spreading on a wetting surface, defined in term of the diameter of the circular wetted area, D , typically follows a power law with time^{17–19} such as

$$D(t) \propto t^n. \quad (7)$$

The time exponent n is found empirically to be around 0.10.¹⁷ However, the classical Hoffman-Tanner-Voinov correlation for capillary spreading is most appropriate for the case of near-perfect wetting ($\theta \approx 0^\circ$). For ink jet-based PCB fabrication, the behavior for the more relevant case of partial wetting ($0^\circ < \theta < 90^\circ$) is less well quantified.

To put these time scales into perspective, a comparison with typical process parameters is useful. UV pinning is commonly used to control ink spreading in graphical printing. By applying an appropriate level of UV light, deposits of UV-curing ink can be partially cured to form a gel or highly viscous liquid very soon after printing in order to retard their spreading, prior to a final curing step further downstream. For a typical commercial ink jet web press in which the substrate moves at 0.5 m/s and a lateral separation of 5 cm exists between the print head and the light source used for pinning, a minimum of 100 ms is required just for the deposited drops to reach the pinning location. It is therefore clear that conventional pinning and curing techniques can have little or no effect on drop spreading during the impact and relaxation phases and would be relevant only in the subsequent capillary phase.

Thermal Considerations

On highly wetting high-energy metallic surfaces, it may be necessary to arrest drop spreading very quickly in order to achieve the required print resolution. While, as shown above, UV pinning and curing may be impossible to achieve within the timescale of the impact and relaxation phases, rapid cooling of the drop can provide a viable alternative process. Either solidification of a phase-change fluid or a very large increase in viscosity, can in principle be achieved in a very short period of time. Phase-change inks which exploit this characteristic are available commercially for both graphic art and printed electronics applications.

Deposition of molten drops at low or moderate Weber number has been well studied.^{3,20,21} A rough estimate of the time scale for solidification can be made by determining the time needed for a deposited molten droplet to lose all of its latent heat and solidify completely. Assuming the thermal conductivity of the substrate to be much greater than that of the molten drop, the solidification time, t_{sol} , may be estimated as

$$t_{\text{sol}} = \frac{D_o^2}{3\alpha_d} \frac{L_f}{C_p(T_m - T_s)}, \quad (8)$$

where α_d , C_p , L_f , T_m , and T_s are the thermal diffusivity, specific heat, latent heat of fusion, melting, and surface temperatures for the molten drop, respectively.²¹ Schiaffino and Sonin scaled this bulk solidification time with the characteristic spreading time in different deposition regimes and derived the following limits:

$$\frac{t_{\text{spr}}}{t_{\text{sol}}} \approx \frac{\text{OhSte}}{\text{Pr}} \quad (\text{Oh} < 0.01),$$

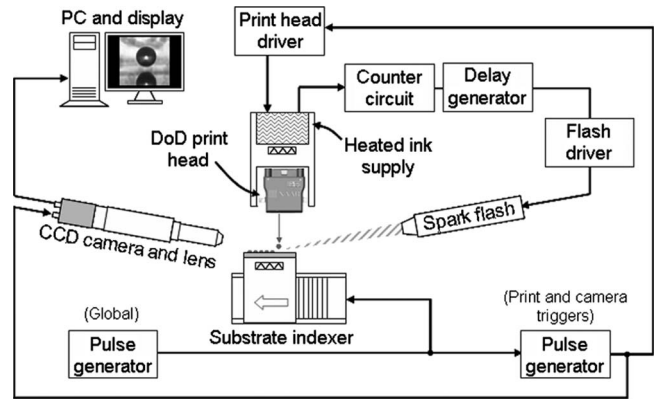


Figure 5. Schematic diagram of the imaging system.

$$\frac{t_{\text{spr}}}{t_{\text{sol}}} \approx \frac{\text{Oh}^2 \text{Ste}}{\text{Pr}} \quad (\text{Oh} > 1), \quad (9)$$

where $\text{Ste} = C_p(T_m - T_s)L_f^{-1}$ and $\text{Pr} = \mu(\rho\sigma)^{-1}$ are the Stefan and Prandtl numbers for the molten drop, respectively.³ It was found that the bulk solidification time was always several orders of magnitudes larger than the drop spreading time, indicating that only a small portion of the drop volume was solidified during the spreading process. However, the effect of surface temperature on molten drop spreading is quite pronounced as reported by various investigators.^{8,20,21} It has therefore been suggested that local solidification at the liquid-solid interface and contact line may instead be the dominating thermal effect.

If heat transfer between the molten drop and the target solid is modeled as that between two semi-infinite bodies brought instantaneously together with negligible interfacial thermal resistance, the thickness s of the solidified layer at the interface grows with time t as²¹

$$s = \sqrt{2t\alpha_d \text{Ste}}. \quad (10)$$

Based on the thermal properties of the phase-change inks used in our experiments and assuming the surface to be at room temperature ($T_s \approx 22^\circ\text{C}$), the solid layer thickness at the end of the impact phase ($t_i = 30 \mu\text{s}$) can be estimated to be about $6 \mu\text{m}$. This rough estimate of solidified layer thickness is independent of drop size, and indeed Bhola and Chandra²¹ found that this local solidification alone was insignificant in affecting the impact phase spreading of millimeter-sized molten drops. However, a greater effect might be expected for the much smaller drops involved in ink jet printing.

APPARATUS AND MATERIALS

Printing was performed with a Xaar XJ126 piezoelectric DoD print head with 126, $50 \mu\text{m}$ -diameter nozzles jetting 80-picoliter ink drops in the system shown schematically in Figure 5. The print head mount had five degrees of freedom of motion (traverse and vertical plus tilting about X-Y-Z axes) and was adapted to incorporate a zoned heating system with a built-in ink reservoir to allow printing of phase-

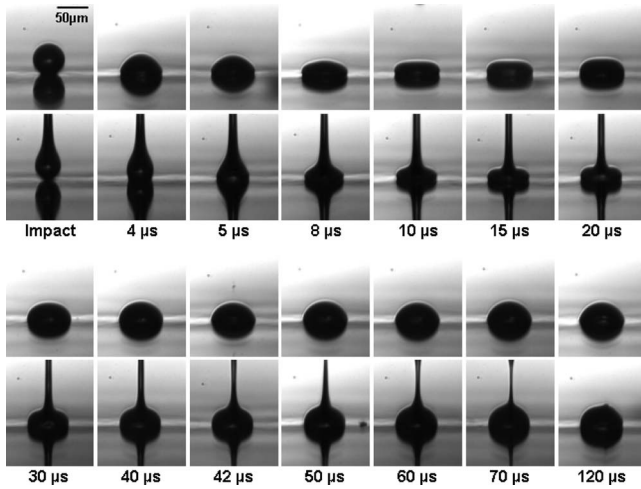


Figure 6. 80 pl UV ink drops deposited on passivated Cu with and without attached ligaments (including reflections).

change inks with melting temperatures up to 100°C. Two inks were used: a UV-curable (UV) ink and a developmental phase-change resist (PCR). All experiments were conducted in a climate-controlled laboratory with stable temperature and humidity. While the room illumination and the flash lamp used for imaging both emitted some light in the UV range of the spectrum, their effect on the UV-curable ink was minimal as it was designed to be reactive only to a very specific UV wavelength. The jetting performance of the Xaar print head was controlled by its proprietary waveform. The only parameter available for user adjustment was the efficiency factor (EFF), which determined the drive voltage of the piezoelectric actuators used for drop ejection. An EFF value of 1.2 was used to achieve a nominal 5 m/s drop velocity, which was verified using double-flash images. Samples of copper-clad FR4 laminates as used in PCB fabrication were used as substrates, with two different surface treatments: passivated or heavily oxidized. The wetting characteristics of the substrates were determined in terms of the apparent ink-substrate contact angles θ_s for sessile ink drops. These drops were formed by depositing roughly 400 pl of ink (five to six drops) on to a substrate sample at room temperature using the Xaar print head; the PCR was deposited in its molten state on to heated substrates maintained at just above the resist's melting temperature. The drop profiles were captured seconds after deposition using the imaging apparatus described below and the values of θ_s were determined by visually fitting the contact angle at the liquid-

solid-air triple point. Since the surfaces were inert and non-absorbent to the ink, penetration was not a factor affecting the contact angle measurement. The ink properties, contact angles, and the dimensionless groups describing the jetting conditions are listed in Table I.

The substrate carrier, which could be electrically heated up to 100°C, was attached to a translation stage driven by a linear servomotor and capable of 5 μm indexing resolution with a maximum velocity of 2 m/s. Initial drop spreading was observed using short-duration (20 ns) flash photography as described previously,^{1,22,23} but with a sensitive monochrome charge coupled device (CCD) camera (Prosilica, EC1020) rather than a digital SLR camera. The optical system provided $<0.5 \mu\text{m}/\text{pixel}$ spatial resolution. The print head command, camera shutter, and flash trigger was synchronized using a Stanford Research System DG535 delay/pulse generator with 5 ps resolution and 1.5 ns accuracy. Therefore, the main source for temporal error came from ink jet jittering. By imaging multiple jetted drops at identical delays after the print command, the maximum positional variation was shown to be around 10 μm . Given the typical drop velocity of 5 m/s, the overall timing uncertainty of the captured images is therefore estimated to be $\sim 2 \mu\text{s}$.

To monitor capillary spreading beyond $\sim 1 \text{ ms}$ after impact, the CCD camera was replaced by a CMOS high-speed camera (Photron 1024 PCI), and the substrate was continuously illuminated with a fiber-optic halogen lamp. In this way the spreading of a single ink drop could be recorded from $\sim 150 \mu\text{s}$ to $>100 \text{ ms}$ after impact, at up to 27,000 fps.

The flash images of the early spreading phases were analyzed using IMAGEJ software with an additional drop shape analysis tool developed by Stalder et al.²⁴ The algorithm locates first the drop-surface interface through reflection and then identifies the drop contour by cubic spline interpolation to determine parameters such as drop diameter and contact angle. Since the algorithm did not assume a spherical cap shape for the deposited drop, it was able to analyze the highly distorted shapes assumed by drops deposited with attached ligaments in the early inertia-driven spreading stage. The high-speed video images of the later capillary spreading phase were processed with custom VISUAL BASIC routines developed in-house. Estimates of drop edge positions using local contrast and information such as pixel counts within the observed drop profiles were extracted from a large number of image frames automatically. By treating the geometry of the spreading drop as a spherical

Table I. Ink properties and experimental condition.

Ink	$\rho(\text{kg}/\text{m}^3)$	$\sigma(\text{N}/\text{m})$	$\mu(\text{Pa}\cdot\text{s})$	We	Oh	$\theta_s(^{\circ})$	$T_m(^{\circ}\text{C})$	$L_f(\text{kJ}/\text{kg})$	$C_p(\text{kJ}/\text{kg}\cdot\text{K})$
PCR	880	0.030	0.012 ^a	24	0.33	8 ^b	70	2.0	0.18
UV	1050	0.026	0.02	45	0.54	11 ^b -25 ^c			

^aValue at jetting temperature of 85°C.

^bOn oxidized Cu surface.

^cOn passivated Cu surface.

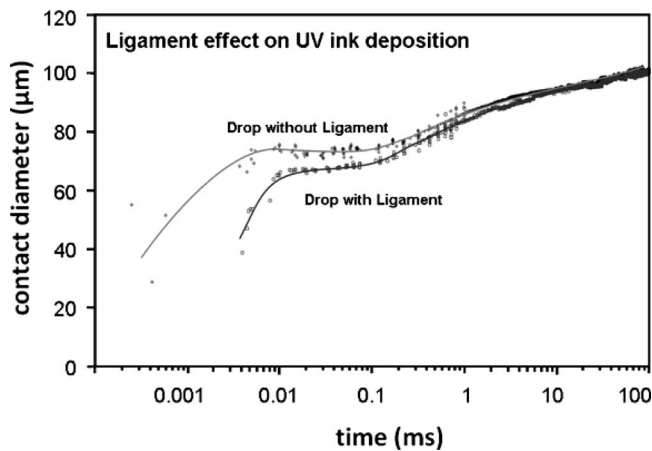


Figure 7. Spreading of UV ink drops deposited with and without ligaments.

cap, estimates could then be made of spreading drop diameters, drop volumes and contact line angles.

RESULTS AND DISCUSSION

Effect of Ligament on Initial Impact

As mentioned above, ink drops jetted from a commercial print head are often accompanied by long attached ligaments. After sufficient time, these ligaments either collapse into the main drops in flight or break up to form satellites. While the behaviors of these ligaments and particularly their roles in satellite formation have been studied before,²³ the effects of ligaments on drop deposition have not been explored.

Deposition of UV ink drops on the passivated Cu surfaces, with and without attached ligaments, is shown in Figure 6. Ligament-free deposition was achieved by increasing the stand-off distance until the ligament had collapsed into the main drop prior to impact. There are notable differences between the deposition behavior with and without ligaments, particularly in the early spreading stage. While the initial postimpact spreading rates were comparable, D_{\max} for drops with ligaments was notably smaller. Slight retraction after D_{\max} was observed for a drop deposited without ligament but was absent in the case with a ligament. As the size of the main drop with attached ligament was significantly smaller, the difference may be attributed to the fact that a significant volume of the jetted fluid was still contained within the ligament at the time of impact. As a result, the effect of impact inertia is expected to be less pronounced.

The time evolution of the drop diameter is plotted in Figure 7. While the time to reach D_{\max}^* , i.e., t_p , is similar in both case (9–11 μs), D_{\max}^* for the drop with ligament was significantly less (1.34 with ligament versus 1.52 without ligament). Although drops deposited under both conditions were oscillation free in the relaxation phase, an average 3% reduction in diameter was observed from 10 to 30 μs after impact for the drops without ligaments. The effect of the ligament on deposition began to diminish after ~ 1 ms. In fact, drops deposited with and without ligaments were observed to spread at similar rates during their respective cap-

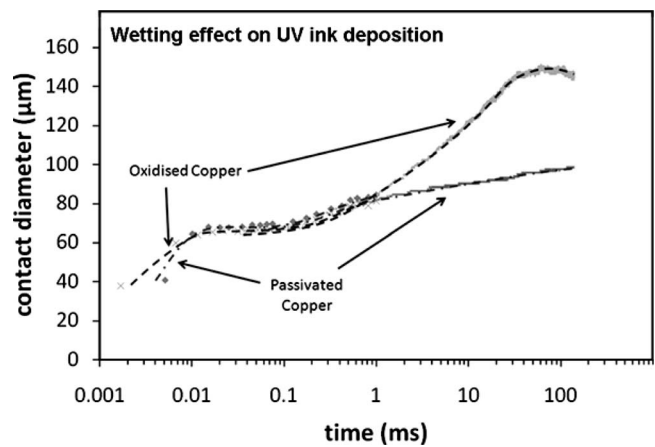


Figure 8. Spreading of UV ink drops on both passivated and oxidized Cu.

illary phases and eventually reached very similar values of D_{equ}^* . Overall, the spreading behavior of drops deposited with attached ligaments was similar to that of smaller or slower drops. Both the smaller D_{\max}^* and the absent of retraction in the relaxation phase are all consistent with a reduction in impact inertia. As the main volume of an impacting drop with ligament is significantly smaller, this simple explanation is intuitively reasonable. However, the actual interaction between the deposited drop and its attached ligament is likely to be more complicated. For example, the fact that the collapsing ligament continues to feed fluid toward the surface while the main drop attempts to retract at the end of the impact phase may be an alternative explanation for the lack of visible retraction during the relaxation phase.

Effect of Wettability: UV-Curable Inks

The spreading of UV-curable ink drops on the oxidized and passivated Cu surfaces (with $\theta_5 = 11^\circ$ and 25° , respectively) is plotted in Figure 8. In both cases, the drops reached D_{\max}^* approximately 20 μs after impact. The values of D_{\max}^* were 1.33 and 1.37 for the oxidized and passivated Cu surfaces respectively, about 4–7% greater than the values estimated from Eq. (2) but within the ranges of reported results.⁵ However in contrast to those observations, subsequent oscillation and reduction in drop diameter were both absent, probably due to the effects of viscosity and surface tension.

While Fig. 7 suggests that the effects of wettability on impact-driven spreading were negligible, there were significant differences between the two substrates during the capillary spreading phase after ~ 1 ms. Spreading on the oxidized Cu was significantly faster, following a power law with a time exponent n of 0.14. A value of $D_{\text{equ}}^* = 2.94$ was reached after 60 ms, about 19% greater than the value of 2.38 estimated from Eq. (3). Notable retraction then occurred after 70 ms. While it is possible that the retraction is related to either surface texture variations or image processing abnormalities, the actual cause is unclear and requires further investigation. Spreading on the passivated surface was significantly slower, with a power law exponent n of approximately 0.06. The drop reached the theoretical value

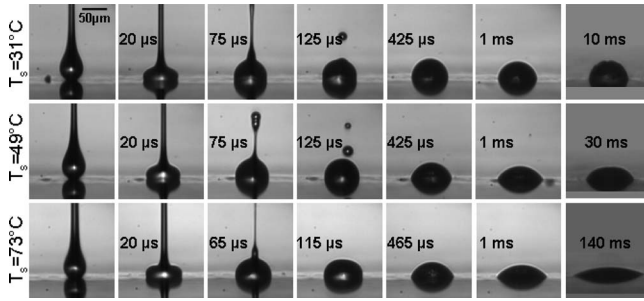


Figure 9. PCR drops depositing on oxidized Cu with different substrate temperatures T_s ; the substrate was moving to the left, giving the observed displacement of the ligaments and satellite drops.

of $D_{\text{equ}}^* = 1.74$ about 80 ms after impact. However, spreading continued after 80 ms and an upper limit was not reached within the period of observation, suggesting a greater than expected value of D_{equ}^* .

The observations of UV ink drops deposited on different wetting surfaces confirm that the postimpact phase oscillation reported in other studies with lower viscosity fluids or larger drops is indeed absent in the ink jet deposition regime.^{5,9} The estimations of D_{max}^* based on Scheller and Bousfield's correlation also agree well with measured values. In addition, the impact phase spreading rates and the values of D_{max}^* are shown to be unaffected by surface wetting, confirming the hypothesis that impact inertia dominates these early deposition characteristics. On the other hand, the impact and relaxation phases of the ink jet deposition process both end within 1 ms after impact and are therefore unaffected by conventional spreading control methods such as pinning and curing. From a process development point of view, the drop spreading behavior in the later, capillary spreading phase is then more important. The capillary spreading on Cu is found to be highly dependent on its surface treatment, and the spreading rate is significantly greater on the more wetting surface. For example, in order to maintain a printed line width of 100 μm on the oxidized Cu surface, Fig. 8 shows that the UV ink drops need to be pinned or cured within 3 ms after deposition. Depending on the available curing power and constraints for the curing lamp placement, meeting this requirement may be difficult in practice.

Effect of Surface Temperature: Phase-change Inks

Figure 9 shows the impact and spreading of drops of PCR on oxidized Cu surfaces with different surface temperatures, T_s . Observations of the images showed that the deformation and spreading immediately after impact were similar, and D_{max}^* was reached in all case after $\sim 20 \mu\text{s}$. The values of D_{max}^* for drops deposited with $T_s = 31$ and 49°C were slightly smaller than those for drops deposited with $T_s = 73^\circ\text{C}$. Minimal retraction and no significant oscillation were observed although small oscillations of the dynamic contact angles (from advancing to receding) were apparent. As in the case of UV-curable ink deposition, the attached ligaments remained visible throughout initial spreading and only collapsed into the deposited drops after $\sim 120 \mu\text{s}$. The

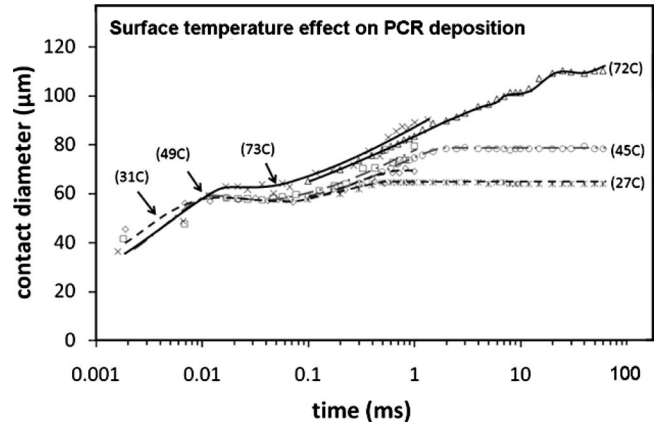


Figure 10. Spreading of PCR drops on oxidized Cu at different T_s .

effect of substrate temperature became more apparent toward the end of the initial spreading. As the temperature increased, the spreading diameter became significantly greater. Complete solidification of the PCR drop deposited with $T_s = 31^\circ\text{C}$ could be identified at 10 ms after impact by the appearance of wrinkles on the upper surface. No such change in drop appearance was observed for $T_s = 49$ and 73°C at equivalent times.

The effect of surface temperature on PCR deposition was demonstrated by combining data from both the flash imaging and high-speed video experiments conducted over three narrow ranges of T_s : 27–31°C, 45–49°C, and 72–73°C, as shown in Figure 10. While spreading immediately after impact was unaffected by T_s , the value of D_{max}^* was slightly temperature dependent ranging from 1.13 to 1.23 as T_s increased from 31 to 73°C. While the observed D_{max}^* for $T_s = 73^\circ\text{C}$ matched well with the value predicted from Eq. (2), values of D_{max}^* for the cooler surfaces were some 10% lower. For $T_s = 31$ and 49°C the drops retracted notably during the relaxation phase. Capillary spreading rates for $T_s = 45$ and 72°C were similar, with power law exponents n of ~ 0.10 . Spreading for $T_s = 27^\circ\text{C}$ was slower with an exponent of 0.07. Drops deposited with $T_s = 72^\circ\text{C}$ did not solidify and continued to spread even after 100 ms, while the spreading of drops with $T_s = 27^\circ\text{C}$ was arrested at 500 μs and with $T_s = 45^\circ\text{C}$ at 2 ms. The final normalized drop diameters, $D_f^* = D_f / D_o$ on the cooler surfaces were measured as 1.25 for $T_s = 27^\circ\text{C}$ and 1.53 for $T_s = 45^\circ\text{C}$, which were significantly smaller than the values predicted from Eq. (3). Spreading of the drops with $T_s = 72^\circ\text{C}$ did not reach an upper limit within the period of observation. The data also showed a slight oscillation of the drop diameter beyond 7 ms after impact. However, since the frequency of oscillation was approximately 50–60 Hz this is likely to have been a result of illumination variations instead of representing real physical behavior.

Complete drop solidification on a cool surface ($T_s = 27^\circ\text{C}$) was observed to occur more than an order of magnitude later in time than the arresting of spreading. It is therefore clear that freezing of the whole of the deposited liquid cannot be responsible for restricting the spreading.

The reduction in D_{\max}^* and the slower capillary spreading rates on the cooler surfaces are both suggestive of greater viscous dissipation. Our observation supports the hypothesis that an increase in fluid viscosity due to the decreasing temperature is the main mechanism for the effect on drop spreading of lowering the surface temperature.²¹ However, empirically quantifying the transient increase in viscosity in these picoliter volumes is difficult. It is easier, and perhaps more useful in term of process development, to quantify the local extent of solidification instead. From Eq. (10), solidification layers at the drop-surface interfaces with $T_s=27$ and 45°C were estimated to be 9 and 11 μm thick at the point at which drop spreading was arrested, respectively. By expanding and rearranging Eq. (10), the surface temperature needed to form a solid layer of thickness s at a given spreading time t_s can be calculated from

$$T_s = T_m - \frac{L_f \rho^2}{2\alpha_d C_d t_s}. \quad (11)$$

While the thickness of the solidified material needed to arrest spreading will clearly depend on the drop size, a value of 10 μm may be used as a reasonable guideline for process development, given the narrow size range of the typical ink jet drops produced from commercial print heads.

CONCLUSIONS

Initial spreading of ink jet drops after impact on passivated and oxidized Cu surfaces was generally free of splashing and excessive oscillation; this can be attributed to the effects of viscous damping. Values of the maximum spread diameter D_{\max}^* were consistent with the predictions of the empirical model of Scheller and Bousfield.¹⁶ While the effect of wettability on impact-driven spreading was negligible, it became significant during the capillary spreading phase. The spreading of UV-curable ink on the more wettable oxidized Cu surface followed a power law with an exponent of 0.14. However, the exponent for the less wettable passivated surface was much lower.

The effect of surface temperature on the spreading of phase-change ink was studied for the oxidized Cu surface. Lowering the substrate temperature appears to be effective in limiting drop spreading and a threshold solidification thickness for arresting ink-jet-sized molten drops has been identified. The variation in drop spreading behavior with substrate temperature was also consistent with an increase in viscous dissipation in the fluid during both the impact and capillary-driven phases of spreading.

ACKNOWLEDGMENTS

This work was co-funded by the Technology Strategy Board's Collaborative Research and Development program,

following an open competition. The Technology Strategy Board is an executive body established by the UK Government to drive innovation. The authors would also like to acknowledge Printed Electronics Ltd. (PEL) and Sun Chemical for their material support and technical assistance.

REFERENCES

- G. D. Martin, I. M. Hutchings, and S. D. Hoath, "Jet formation and late-stage ligament instability in drop-on demand printing", *Proc. IS&T's NIP 22* (IS&T, Springfield, VA, 2006) pp. 95–98.
- A. M. Worthington, "On the form assumed by drops of liquids falling vertically on a horizontal plate", *Proc. R. Soc. London, Ser. A* **25**, 261–272 (1876).
- S. Schiaffino and A. A. Sonin, "Molten droplet deposition and solidification at low Weber numbers", *Phys. Fluids* **9**, 3172–3187 (1997).
- K. K. B. Hon, L. Li, and I. M. Hutchings, "Direct writing technology: Advances and developments", *CIRP Ann.* **57**, 601–620 (2007).
- H. Dong, W. W. Carr, and D. G. Bucknall, "Temporally-resolved ink jet drop impact on surfaces", *AIChE J.* **53**, 2606–2617 (2007).
- A. P. Newbery and P. S. Grant, "Droplet splashing during arc spray of steel and the effect on deposition microstructure", *J. Therm. Spray Technol.* **9**, 250–258 (2000).
- D. B. Van Dam and C. Le Clerc, "Experimental study of the impact of an ink jet printed droplet on a solid substrate", *Phys. Fluids* **16**, 3403–3414 (2004).
- D. Attinger, Z. Zhao, and D. Poulikakos, "An experimental study of molten microdroplet surface deposition and solidification: transient behavior and wetting angle dynamics", *ASME Trans. J. Heat Transfer* **122**, 544–556 (2000).
- R. Rioboo, M. Marengo, and C. Tropea, "Time evolution of liquid drop impact onto solid, dry surfaces", *Exp. Fluids* **33**, 112–124 (2002).
- S. Chandra and C. T. Avedisian, "On the collision of a droplet with a solid surface", *Proc. R. Soc. London, Ser. A* **432**, 13–41 (1991).
- M. Pasandideh-Fard, Y. M. Qiao, S. Chandra, and J. Mostaghimi, "Capillary effects during droplet impact on a solid surface", *Phys. Fluids* **8**, 650–659 (1996).
- T. Mao, D. C. S. Kuhn, and H. Tran, "Spread and rebound of liquid droplets upon impact on flat surfaces", *AIChE J.* **43**, 2169–2179 (1997).
- J. Fukai, M. Tanaka, and O. Miyatake, "Maximum spreading of liquid droplets colliding with flat surfaces", *AIChE J.* **31**, 456–461 (1998).
- I. V. Roisman, R. Rioboo, and C. Tropea, "Normal impact of a liquid drop on a dry surface: model for spreading and receding", *Proc. R. Soc. London, Ser. A* **458**, 1411–1430 (2002).
- A. Asai, M. Shioya, S. Hirasawa, and T. Okazaki, "Impact of an ink drop on paper", *J. Imaging Sci. Technol.* **37**, 205–207 (1993).
- B. L. Scheller and D. W. Bousfield, "Newtonian drop impact with a solid-surface", *AIChE J.* **41**, 1357–1367 (1965).
- L. H. Tanner, "The spreading of silicone oil drops on horizontal surfaces", *J. Phys. D* **12**, 1473–1484 (1979).
- R. Hoffman, "A study of the advancing interface. I. Interface shape in liquid-gas systems", *J. Colloid Interface Sci.* **50**, 228–241 (1975).
- O. V. Voinov, "Hydrodynamics of wetting", *Fluid Dyn.* **11**, 714–721 (1976).
- R. Li, N. Ashgriz, and S. Chandra, "Deposition of molten ink droplets on a solid surface", *J. Imaging Sci. Technol.* **52**, 020502 (2008).
- B. Bhola and S. Chandra, "Parameters controlling solidification of molten wax droplets falling on a solid surface", *J. Mater. Sci.* **34**, 4883–4894 (1999).
- I. M. Hutchings, G. D. Martin, and S. D. Hoath, "High speed imaging and analysis of jet and drop formation", *J. Imaging Sci. Technol.* **51**, 438–444 (2007).
- S. D. Hoath, G. D. Martin, R. Castrejon-Pita, and I. M. Hutchings, "Satellite formation in drop-on-demand printing of polymer solutions", *Proc. IS&T's NIP23* (IS&T, Springfield, VA, 2007) pp. 331–335.
- A. F. Stalder, G. Kulik, D. Sage, L. Barbieri, and P. Hoffmann, "A snake-based approach to accurate determination of both contact points and contact angles", *Colloids Surf., A* **286**, 92–103 (2006).